

Strong-coupling of WSe₂ in ultra-compact plasmonic nanocavities at room temperature

Marie-Elena Kleemann¹, Rohit Chikkaraddy¹, Evgeny M. Alexeev², Dean Kos¹, Cloudy Carnegie¹, Will Deacon¹, Alex de Casalis de Pury¹, Christoph Grosse¹, Bart de Nijs¹, Jan Mertens¹, Alexander I Tartakovskii², Jeremy J Baumberg^{*,1}

¹ NanoPhotonics Centre, Cavendish Laboratory, University of Cambridge, Cambridge, CB3 0HE, UK

² Department of Physics and Astronomy, University of Sheffield, Sheffield S3 7RH, UK

KEYWORDS: room temperature strong-coupling, 2D materials, TMDs, plasmons, polaritons, plexcitons, nanoparticle on mirror

ABSTRACT:

Strong-coupling of monolayer metal dichalcogenide semiconductors with light offers encouraging prospects for realistic exciton devices at room temperature. However, the nature of this coupling depends extremely sensitively on the optical confinement and the orientation of electronic dipoles and fields. Here, we show how plasmon strong coupling can be achieved in compact robust easily-assembled gold nano-gap resonators at room temperature. We prove that strong coupling is impossible with monolayers due to the large exciton coherence size, but resolve clear anti-crossings for 8 layer devices with Rabi splittings exceeding 135 meV. We show that such structures improve on prospects for nonlinear exciton functionalities by at least 10^4 , while retaining quantum efficiencies above 50%.

Transition metal dichalcogenide (TMD) semiconductor heterostructures open up many possibilities for photonics. Of major interest is the strong binding energy of their excitons which allows for room temperature exciton devices¹⁻³, thus preferable to traditional III-V GaAs-based heterostructures where excitons ionize at 300K. When such strong excitonic dipoles are embedded in optical resonators, the resulting modified optical density of states changes their emission lifetime through the Purcell factor⁴⁻⁷. In extreme cases, when the light-matter coupling is strong enough, the regime of Rabi oscillations and strong coupling is reached, where the excitons and photons form new mixed polariton states. These exhibit many compelling features including Bose condensation⁸⁻¹⁰ with superfluid characteristics¹¹ and a wide range of applications such as low-energy switching^{12,13} and tuneable low-threshold semiconductor lasing¹⁴.

So far, the optical resonators used with TMDs are based on dielectric or metal mirrors, and assisted by cryogenic cooling of monolayers to obtain strong coupling^{15,16}. Often spectral splittings¹⁷⁻¹⁹ are barely resolved and are on the order of thermal energies. In order to access many of the key features, clearly resolved polaritons are demanded with splittings >100meV at room temperature. Since the light-matter interaction depends inversely on the

* jjb12@cam.ac.uk

cavity volume, $g \propto 1/\sqrt{V}$, compact optical modes are favoured for nonlinear optical and switching devices. To significantly improve on dielectrically-confined light (with minimum volume $V_{\min} \sim (\lambda/n)^3$ in refractive index n), plasmonic resonators are required²⁰. Gap plasmons allow us to reach optical volumes below 50nm^3 straightforwardly²⁰, even below 1nm^3 in certain cases²¹. However in such extreme plasmonic cavities the resonant optical field is typically polarised perpendicularly to the layer planes^{22,23} and hence poorly coupled to the exciton dipole which is oriented in-plane²⁴ (see experiments in S5,6). This suggests that strong coupling of TMDs in plasmonic cavities is problematic, in comparison to systems with dipoles oriented out-of-plane²⁵⁻²⁷. One approach is to use Type-II stacked TMD bilayers to create dipolaritons, but these are currently challenging to fabricate

Here we present a different approach to TMD-plasmon interactions, which is capable of room-temperature strong coupling in ultra-compact resonators with Rabi splittings exceeding $\Omega_R > 140\text{meV}$. We show that the high refractive index ($n \sim 3$) of TMD layers retunes the plasmons so that thicker gap cavities are required to reach appropriate resonance conditions. Surprisingly, we show that multilayers ($N_L \sim 8$) of WSe_2 achieve this strong coupling, despite their typically weak luminescence from exciton recombination, which is indirect. We explain this strong coupling by the dramatic Purcell enhancements in the plasmonic cavities, which competes with carrier scattering so that optical re-emission overcomes phonon-driven intervalley transfers. This localised plasmonic geometry thus provides a route to unusual nonlinear optics (for instance also based on spin/valley-selection) as well as to accessing photon blockade effects at room temperature.

Results

Construction of plasmon-coupled TMDs

Vertically-stacked atomically-thin materials exhibit a wide range of optical and electrical properties. Semiconductor TMDs such as MoS_2 and WSe_2 have strong excitons in the visible and near-IR with spin-selective excitation into K, K' valleys^{28,29}. Monolayers become direct-gap and produce strong exciton photoluminescence (PL) which is suppressed as soon as $N_L \geq 2$. In strong coupling, the exciton emission rate has to exceed both the cavity loss rate κ and the exciton scattering rate $\gamma_x \geq k_B T$. TMDs are suited because plasmonic cavities with low $Q \sim 20$ match their typical scattering rates at room temperature. In this regime, excitons with oscillator strength f give Rabi splitting $\Omega_R \propto \sqrt{f N_L n / \lambda^3}$. Since the band structure of TMD multilayers changes from that of monolayers when they are van-der-Waals stacked, we expect that layers must be spaced (for instance with hBN ¹⁶) to retain efficient emission, increasing the cavity volumes and reducing their Rabi coupling.

A second problem is the tuning of the different plasmon modes in nanometre-scale gap cavities. Smaller gaps d result in tighter plasmonic confinement ($V \sim d^2 D$ for nanoparticles of diameter D) however the resonant modes rapidly red-tune to the infrared, out of resonance with the excitons. This is a particular problem for cube nanoparticle geometries, which have been used to produce enhanced Purcell factors when coupled to semiconductor quantum dots⁴ or MoS_2 ³⁰, but only for gaps of order $d \sim 10\text{nm}$. We recently showed that truncated spherical nanoparticles (as produced naturally by the equilibrium faceting) are optimal to produce strong coupling in the visible/near-IR³¹. Here, we balance the gap size with the TMD refractive index to achieve optimal strong coupling conditions.

Our self-assembled plasmonic cavities use the nanoparticle-on-mirror geometry (NPoM) to embed exfoliated WSe₂ multilayers of increasing N_L inside the gap. Briefly, TMD layers are transferred to template-stripped Au substrates and Au nanoparticles of different diameter $D = 60\text{-}100\text{nm}$ are drop-cast on top to form NPoMs. These are spaced far enough apart ($>5\mu\text{m}$) to observe them individually. Image charges induced in the underlying Au film plasmonically couple each faceted nanoparticle with its mirror image, enclosing a nanocavity and creating a system resembling the coupled plasmon dimer (Fig.1a,b). Resonance with the A -exciton is achieved by tuning the cavity resonance for different gap thicknesses by selecting D . White-light dark-field (DF) microscopy, with light incident at high angles ($|\theta|>55^\circ$) and collected at lower angles, is then used to identify the plasmonic resonances (Fig.1c,d) and resolve the hybrid plasmon-exciton branches for single NPoM cavities.

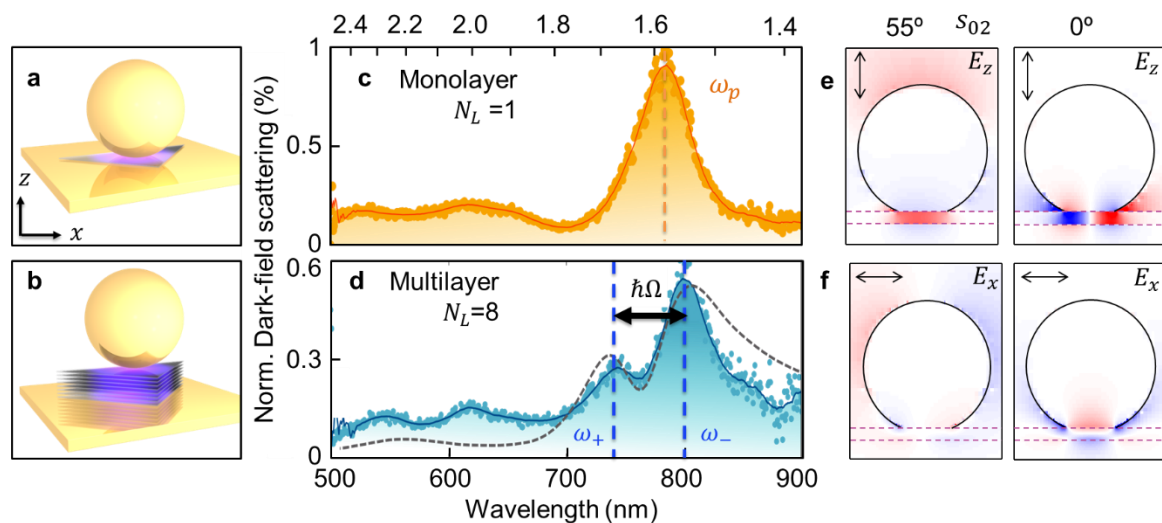


Figure 1 | Optical signature of single and multilayer WSe₂ embedded in plasmonic nanocavities. (a,b) Schematic of nanoparticle-on-mirror cavity encapsulating WSe₂ flakes for $N_L=1,8$. (c,d) Dark-field scattering of individual NPoMs showing single plasmon peak for $N_L=1$ WSe₂, but a mode splitting due to strong coupling for multilayer $N_L=8$ reproduced by FDTD simulations (dashed line). (e) Simulated field distributions $E_{x,z}$ for two plasmon coupled modes (s_{02}, s_{11}) at $\lambda=780$ nm with high refractive index material (dashed) in the 10 nm gap ($n=2.8$). Angles of incidence 55° (left) and 0° (right); red-blue colour-scale shows field enhancements of $\pm 30 |E_0|$.

For $D=100\text{nm}$ NPoMs, the dominant coupled plasmon resonance λ_p in the system is beyond 700nm (shorter λ resonances correspond to transverse and quadrupoles with weaker field confinement and enhancements), set by the exact geometry³². In these nanocavities, field enhancements up to $|E|/|E_0| \approx 70$ inside the high n layer (Fig.1e) should yield Purcell factors sufficient to produce strong coupling³³. Incorporating $N_L=1$ MoS₂ or WSe₂ monolayers in such nanogaps, and observing them by using dynamic tuning of the plasmons (SI Fig.S5) *always* however gives weak coupling only, merely enhancing photoluminescence yields by up to 5-fold when on resonance (note off-resonance also enhanced in such gaps).

Strong coupling in WSe₂ flakes

By instead incorporating thicker WSe₂ flakes, we clearly observe the appearance of strong coupling (Fig.1d). Instead of a single plasmon mode, a splitting between two exciton-plasmon-polaritons (or ‘plexcitons’) is seen, with peak separations between ω_+ and ω_- exceeding 140meV. In this case, an exfoliated flake of thickness 10nm with $N_L=8$ layers

spaces the Au plasmonic gap (Fig.2a,b). This generates strong infra-red plasmonic resonances (appearing red in Fig.2a) as compared to the NPoM systems produced off the flake which appear green. Atomic force microscopy (AFM) confirms the multilayer thickness (Fig.2c), which gives a reflection spectrum matching that expected from the permittivity of WSe₂ (see SI Fig. S2) and appearing purple in bright field. At room temperature, the large exciton binding energy (400meV) in WSe₂ results in stable excitons with photoluminescence at the *A*-exciton. This emission is linear in excitation power, with no shifts, indicating little influence from screening or charging (Fig.2d). The exciton peak at $PL_{xA}=780$ nm and its strength agrees with literature^{28,29,34–36}.

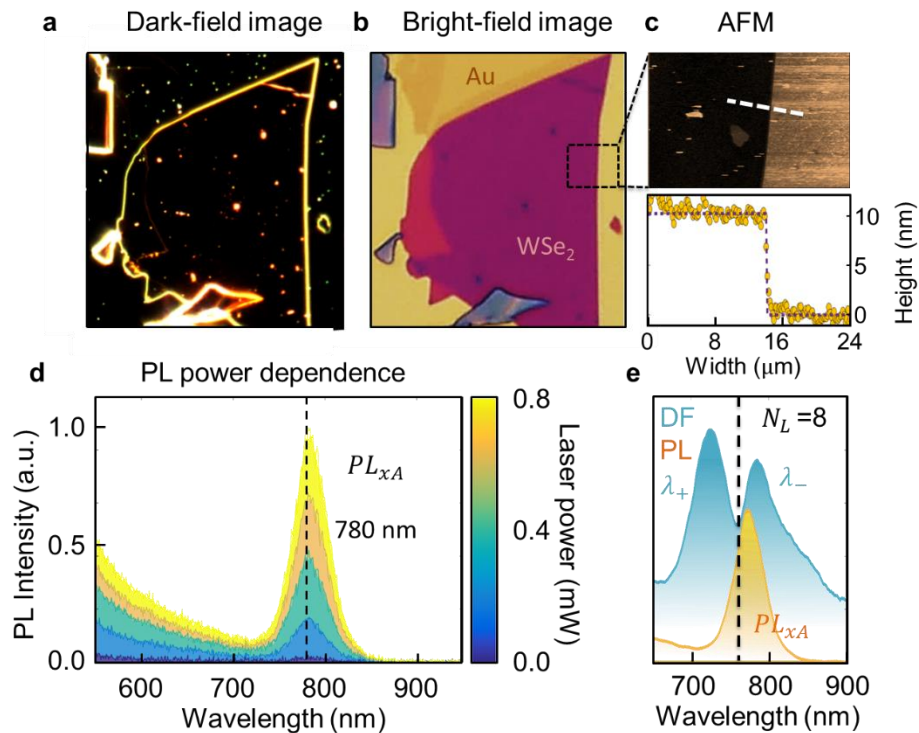


Figure 2 | WSe₂ stack properties. (a) Dark-field, (b) Bright-field, and (c) AFM images of multilayer WSe₂ stack. AFM height profile of flake edge (white line) gives $d=10\pm 0.4$ nm, corresponding to 8 layers. (d) Power-dependent PL emission at room temperature of the WSe₂ stack (away from NPoM). Dashed lines mark PL from *A* exciton. (e) Scattering and PL emission spectra on same NPoM, dashed line gives exciton absorption peak.

Tunable plasmonic cavity with high Purcell factor:

TMDs switch from direct to indirect band gaps when moving from single- to multi-layers^{36,35}. Here we show that by matching the plasmon resonance to the direct *A*-exciton transition in multilayers, we resonantly enhance the radiative decay process at the *K*, *K'* points, speeding it up by more than an order of magnitude. Although in multilayer WSe₂ the direct *K*-*K* exciton is at 1.63 eV, far above the Γ -*K* transition energy at 1.4 eV (Fig. S1),³⁵ intervalley relaxation requires phonon interactions that take only ~ 30 fs at 300K³⁷. Embedding the WSe₂ in plasmonic cavities with very high Purcell factor and tuning the plasmon resonance to match the *A*-exciton transition selectively enhances their radiative recombination (below their undressed radiative recombination time of ~ 200 fs³⁷), thus switching on the strong coupling even for multilayer WSe₂.

The clear presence of the flake sandwiched within the plasmonic gap is shown by surface-enhanced Raman scattering (SERS) of the assembled NPoMs. When pumped at 633nm, typical Raman modes of bulk WSe₂ are observed (SI Fig.S7), showing that it remains intact and is not chemically modified by the interaction with the Au or by laser irradiation. Comparing the DF scattering spectra with the PL spectra on the same NPoM shows that the latter is red-shifted from the DF dip position, matching the typical 20 nm Stokes shifts found in WSe₂ arising from relaxation^{5,19}. Strong coupling thus confirms that re-emission from the A-exciton happens here before phonon scattering can occur.

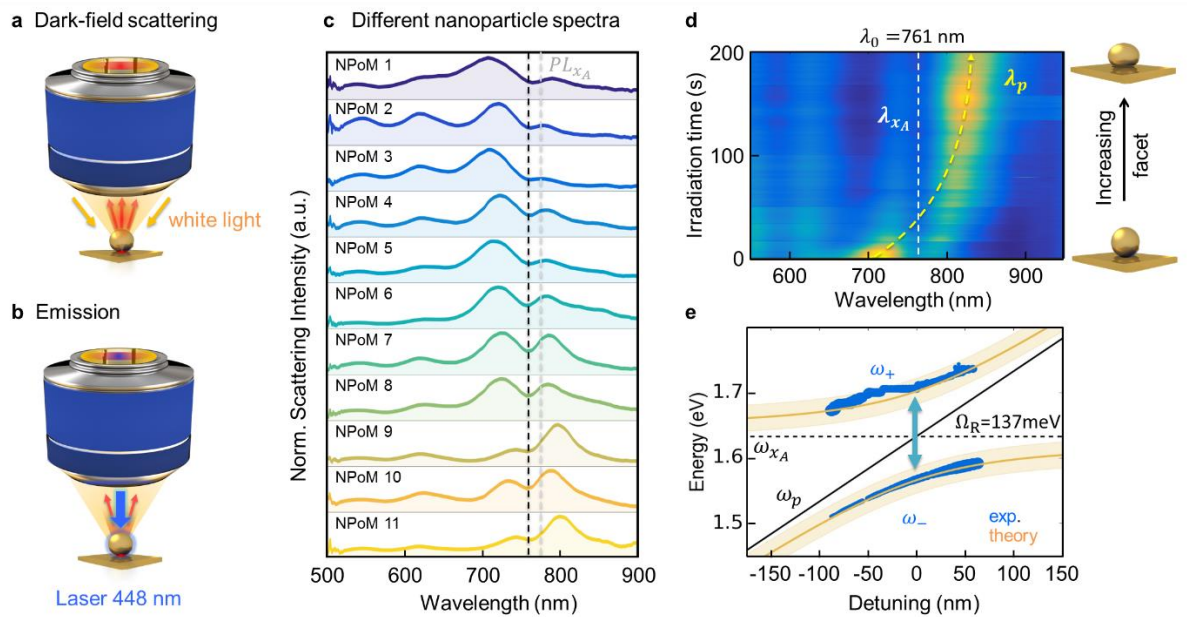


Figure 3 | Signature of strong coupling in individual NPoM constructs. (a) White-light dark-field scattering, and (b) PL/irradiation setups. (c) Normalized dark-field scattering spectra of individual NPoM constructs each with $N_L=8$ WSe₂ spacer, black dashed line at A-exciton position. (d,e) Laser-induced tuning of NPoM plasmon resonance via growth of lower facet, mapping out anti-crossing around A-exciton. (e) Hybrid plasmon-exciton branches ('plexcitons', ω_{\pm}) with Rabi-splitting $\Omega_R = 137$ meV. Blue dots correspond to extracted experimental values and orange to coupled oscillator model.

Evidence of strong coupling

Dark-field scattering spectra are measured on many individual NPoM constructs with $N_L=8$ layers of WSe₂ as a spacer material (Fig.3). The different normalised scattering spectra (Fig. 3c) all show consistent double-peaked spectral features with a characteristic dip at the position of the A exciton. The slight tuning of the plasmon modes arises from variations in the NP sizes and facets³⁹, which in the strong coupling regime then produces different relative peak heights as observed. No Fano-like lineshapes are seen, corroborating the regime of strong coupling⁴⁰. By contrast, for WSe₂ monolayer constructs ($N_L=1$), which scale down both the total oscillator strength and the cavity volume, no such dips are seen.

Although plotting different spectra from NPoMs traces out the anti-crossing, we can also tune a single NPoM coupled plasmon resonance so that it tunes across resonance with the A-exciton. To do this, we use blue-irradiation of the NPoM (0.1mW of a 448 nm CW laser) to drive Au atoms towards the NP bottom facet, which red-tunes the plasmon, ω_p (SI Fig.S3) as

previously studied⁴¹. The robust WSe₂ layers prevent any metal-bridging from NPs onto the bottom mirror, while SERS confirms that the WSe₂ remains intact throughout. A clear anti-crossing is also seen in this case (Fig.3d,e), which can be fit to the semi-classical coupled oscillator model^{20,42} giving

$$2\omega_{\pm} = (\omega_p + \omega_{xA}) \pm \sqrt{\Omega_R^2 + \delta^2}, \quad (1)$$

where $\delta = \omega_p - \omega_{xA}$ is the detuning (also extracted from the fits), and each plasmon resonance position (black line) is extracted from the two peak positions. Comparing this oscillator model (orange) with the experimental results (blue) shows good agreement (Fig. 3e). The two hybrid plexcitons exhibit the characteristic plasmon-exciton dispersion with Rabi splitting of 137 meV. The same Rabi splitting is found for all the NPOMs here (Fig.3c), showing the consistency of the cavity volume and oscillator strength at different spatial locations, and the robustness of this effect. Despite the small cavity volume, the splitting is large because the Q-factor of these cavities is well matched to the exciton linewidth, thus maximising the Rabi coupling, $\Omega_R = \sqrt{g^2 - (\gamma_x - \kappa)^2}$ by minimising $\gamma_x - \kappa$.^{19,42-44} We also note that $\Omega_R > (\gamma_x + \kappa)/2$ as required for strong coupling.

Plasmon mode tuning

To better understand the system, we use finite-difference time-domain (FDTD) simulations to calculate the mode volume V and the Purcell Factor $F_P \propto Q/V$ (Fig.4). Because TMDs are highly anisotropic (with non-resonant n which is 50% times smaller along z - compared to in-plane), their mode tuning depends sensitively on field orientations (Fig.4b,1e). With their large out-of-plane refractive index $n_z=2.8$,³⁴ the lowest gap plasmon is red-shifted to $\lambda \approx 800$ nm even for these large 10nm gaps (Fig.4b). The two resonances seen when exciton contributions are switched off (leaving just the non-resonant n) have different polarisation selection rules, and are seen either at high angles (z , s_{02}) or normal incidence (x , s_{11}), according to their symmetry (Fig.4b,1e).

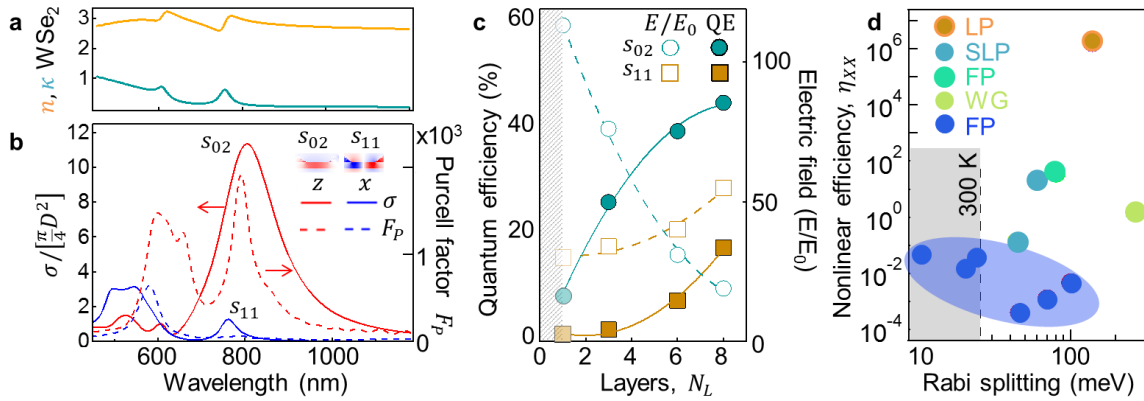


Figure 4 | Comparison of calculated Purcell and pumping factors. (a) Effective refractive index $n + i\kappa$ of multilayer WSe₂. (b) FDTD simulations of the scattering cross section (solid lines) and Purcell factors (dashed) for optical fields along normal (z) and in-plane (x) directions. (c) Quantum efficiency (solid lines) and field enhancement (dashed) vs number of monolayers, when keeping s_{02} , s_{11} tuned to A -exciton by changing the NP diameter (see SI9). (d) Comparison of strong-coupling Rabi splittings and exciton nonlinear efficiencies for different cavities: localised plasmon (LP, present work), surface lattice plasmons (SLP), Fabry-Perot mirror cavities (FP, blue=monolayer, green=multilayer), waveguide (WG) [for references see SI Table S9].

These symmetries become crucial when considering not point dipole emitters such as molecules²⁰, but spatially-delocalised excitons. The exciton coherence diameter d_c is given by⁴⁵

$$d_c = 8\hbar \sqrt{\frac{\pi}{M\Delta}}, \quad (2)$$

where the total exciton mass $M = m_e^* + m_h^* = 0.63m_e$ ⁴⁶ and the exciton homogeneous spectral linewidth at room temperature is $\Delta=40\text{meV}$ ³⁷, resulting in $d_c = 24 \text{ nm}$ for WSe₂. This means that the s_{11} excitation (in Fig.1e, top right) is suppressed since it tries to drive dipoles that are only 20 nm apart with opposite phase within the same exciton. For this reason in our NPoM system, the s_{02} mode dominates exciton coupling⁴⁷.

The Purcell factors here reach $F_p \lesssim 2000$ near 800 nm, speeding up radiative decay from the K, K' excitons sufficiently to allow strong coupling before intra-valley scattering occurs. While the E_x field strengths aligned to the dominant in-plane exciton⁴⁸ dipole orientation are insufficient to retrieve strong coupling, in multilayers the exciton has an out-of-plane component. Using the in-plane refractive index $n_x(\lambda)$ constrained by fitting the reflectivity of the flake away from NPoMs (Fig.S2), we estimate that this exciton dipole strength along z is of order 25% of the x -dipole for multilayers. Such mixing likely originates from multilayer-induced mixing (evidenced in polarisation-dependent in-plane reflectivity measurements³⁴), as stress-induced band mixing is not evident (the SERS phonon lines are found to be unshifted).

For monolayer plasmon cavities, several factors prevent strong coupling. The exciton dipole is now completely in-plane and cannot couple to the strong E_z fields. Secondly, the much smaller monolayer gap red-shifts the fundamental plasmon resonance far beyond the exciton into the IR, requiring plexciton coupling through higher-order plasmon modes. Since these possess oscillatory fields in the gap (Fig.S6), they also cannot couple to the delocalised exciton because of destructive interference as described above, despite their strong field enhancements. If instead monolayers are placed inside wider plasmon gaps to retune the lowest plasmon back to the exciton resonance³⁰, then the larger cavity volume contains too little exciton oscillator strength to reach strong coupling. Alternatively, reducing the nanoparticle size to tune the plasmon to match the exciton resonance, gives also too small a field enhancement (Fig.4c). The optimal number of WSe₂ layers thus depends on the largest field strength that can be obtained while retuning the lowest plasmon mode into exciton resonance (Fig.4c).

Finally, we comment on the comparison with dielectric-based TMD strong coupling, focussing on how exciton-exciton nonlinearities will work in each system, by identifying an appropriate figure of merit. While the Rabi energy is one key parameter, the nonlinear properties of such systems depend on the exciton density because the underlying Coulombic-interaction depends on the exciton density squared. This scales with the spatial overlap of the confined optical field with the excitonic material component, set by what fraction of each cavity round trip that the light spends as an exciton. Given optimal tuning (as in Fig.3c-e), this nonlinear scaling is controlled by both the cavity field enhancement and the fraction of the light that is inside the semiconductor layers, $F_X = V_X/V$ where V_X is the volume of the optical mode which overlaps with the TMD layers (see Theory). For reports in

the literature of TMD strong coupling (Table S8), we can thus map this exciton nonlinear efficiency, $\eta_{XX} = (F_P F_X)^2$, which varies by more than 8 orders of magnitude in different constructs (Fig.4d). The extreme confinement within the plasmonic cavity here, and its complete filling with TMD layers, thus produces a system which is extremely favourable for nonlinear device performance.

Conclusion

We have successfully shown how ultra-compact plasmonic resonators in combination with TMDs are capable of reaching the strong coupling regime at room temperature with Rabi-splittings exceeding $\Omega_R > 140\text{meV}$. Drastic Purcell enhancement of plasmonic cavities dominates over carrier scattering and phonon-driven intervalley transfers. The simple tuneability of the NPoM geometry allows for optimal coupling in extremely compact cavities with ultrasmall mode volumes. Three considerations are crucial: (i) the coherence size of the exciton compared to the plasmonic mode, (ii) the orientation of the exciton dipole which is exactly in-plane in monolayers, but 25% out-of-plane in multilayers, and (iii) the radiative coupling which needs to be larger enough without tuning the plasmon far into the infrared. Our success opens up new routes to create low-energy photonic devices such as low-threshold lasers and optoelectronic all-optical circuit elements including polariton switches, transistors and logic gates at room temperature.

Methods:

Sample fabrication:

Monolayer and few-layer TMD flakes are mechanically exfoliated from bulk crystals onto a silicon substrate coated with a polymer bilayer (100 nm PMGI and 1 μm PMMA). The top PMMA layer with a chosen crystal is lifted off the substrate by dissolving the sacrificial PMGI layer and transferred onto a gold substrate. The PMMA membrane is dissolved in acetone, and the sample is rinsed in isopropanol and dried with a nitrogen flow.

Gold substrates are fabricated by template stripping: a 100 nm Au layer is evaporated onto polished silicon wafers. Small silicon substrates (10x10 mm²) are glued to the Au surface using epoxy glue (*EPOTEK377*). In order for the epoxy glue to cure, the samples are left on a hot-plate for 2h at a temperature of 150°C. After the samples cool, the Au substrates are stripped by peeling the top silicon substrates off, leaving flat Au adhering to the small Si squares.

Nanoparticles (60-100 nm citrate stabilised Au, BBI Scientific) are assembled directly onto Au substrates covered at low density with WSe₂, MoSe₂ or MoS₂ flakes. Remaining colloidal particles are removed by washing with deionised water, and the samples then dried with nitrogen gas.

Dark-field and emission spectroscopy:

A customised dark-field microscope (Olympus BX51) is used to perform white-light dark-field and emission spectroscopy of individual NPoMs. An incandescent light source is focused with a 100x dark-field microscope objective providing high angle illumination up to 69° (NA=0.93). The numerical aperture to collect the scattered light is NA=0.8 (Fig. 3a). Using a confocal geometry in collection, the scattered light is collected with a 50 μm -diameter fibre as a pinhole to limit the collection area on the sample (1 μm diameter). Spectra are

recorded with a cooled spectrometer (Ocean Optics QE65000) with integration times of 1000 ms.

For emission spectroscopy, individual NPoMs are illuminated with a single-mode fiber-coupled diode laser (Coherent CUBE) at 448 nm pump wavelength. Collimated laser light fills the back-focal-plane of the microscope objective, thus illuminating in bright-field a diffraction-limited area of 360 nm diameter on the sample. In order to avoid damage the particles are irradiated with powers below 0.1 mW (corresponding to power densities $< 0.4 \text{ mW}\mu\text{m}^{-2}$) at the sample. The emitted light is recorded with the same spectrometer as for the white light spectroscopy, with the laser light blocked by a 500 nm long-pass filter (Thorlabs) in the collection path.

Theory:

Full-wave finite difference time domain (FDTD) simulations are performed to calculate the plasmon cavity resonances for a 100 nm spherical gold nanoparticle (AuNP) with 40 nm bottom facet diameter (as all nanoparticles are faceted^{49,50}). Au NPs are placed above the 100nm-thick Au mirror with a $d=1\text{-}10$ nm gap. The wavelength-dependent refractive index of the gap was extracted from the experimental reflectivity spectrum of the same WSe₂ flake (Fig. 4a), and these parameters incorporated into full-wave calculations to model the NPoM cavity. The Au NP was illuminated with an s- or p-polarized plane wave (TFSF source) from an angle of incidence of $\theta_i=55^\circ$ or 0° (which are known to couple to z or x,y cavity modes). The inbuilt sweep parameter was used to sweep the incident wavelength from 500 to 900 nm. The scattered light for each wavelength was collected within a cone of half angle $\theta_c=55^\circ$ based on the numerical aperture of the objective. Since the cavity resonance is sensitive to the facet size, this is tuned to scan the plasmon across the exciton resonance.

To estimate the mode volume of the cavity resonance, the Purcell factor was calculated,

$$F_P = \frac{3}{4\pi^2} \left(\frac{\lambda_0}{n} \right)^3 \frac{Q}{V}. \quad (4)$$

This Purcell factor describes the enhanced spontaneous decay rate of a classical dipole in the NPoM cavity, and is simulated by placing dipoles in specific orientations either in the centre of the facet or at the edge, near the top nanoparticle where the fields are most strongly enhanced (Fig.1e,4). From this, and the Q-factor extracted from the resonant lineshape of each mode, the volume was then extracted.

To simulate the strong coupling, the gap of NPoM cavity is modelled as a self-consistent dispersive medium with excitonic dielectric permittivity described by the Lorentz model as

$$\varepsilon_{\text{tot}}(\omega) = \varepsilon_\infty + \sum_j \frac{f_j \omega_j^2}{\omega_j^2 - \omega^2 - i\gamma_j \omega}, \quad (5)$$

where $\varepsilon_\infty = 5$ is the non-resonant background, and for each exciton (A, B, C) f_j is the reduced oscillator strength, $\hbar\omega_{A,B} = 1.63, 2.0$ eV are the A, B exciton energies with linewidth parameters $\gamma_{A,B} = 70, 100$ meV. The f_j are tuned to match the experimentally observed reflectivity and strong coupling spectra. This permittivity has a 50% reduced background refractive index for fields normal to the layer planes, with the anisotropy in f_j matched to the experimental data.

The exciton nonlinear response depends on local exciton Coulomb interactions, and thus is proportional to n_X^2 (for exciton density n_X). The light intensity in the cavity is proportional to Q , giving $n_X \propto \frac{Q}{V_x} = \frac{Q}{V} \frac{V}{V_x} = F_P F_X$ with $F_X = V/V_x$. A suitable figure of merit is then $\eta_{XX} = (F_P F_X)^2$.

Acknowledgment: We acknowledge support from EPSRC grants EP/G060649/1, EP/L027151/1, EP/G037221/1, EPSRC NanoDTC, and ERC grant LINASS 320503. J.M. acknowledges support from the Winton Programme of the Physics of Sustainability. R.C. acknowledges support from the Dr. Manmohan Singh scholarship from St John's College, University of Cambridge. AIT and EMA acknowledge support from EPSRC grant EP/M012727/1

References:

1. Britnell, L. *et al.* Strong Light-Matter Interactions in Heterostructures of Atomically Thin Films. *Science*. **340**, 1311-4 (2013).
2. Lundt, N. *et al.* Monolayered MoSe₂ : a candidate for room temperature polaritonics. *2D Mater.* **4**, 15006 (2016).
3. Wang, Z. *et al.* Giant photoluminescence enhancement in tungsten-diselenide-gold plasmonic hybrid structures. *Nat. Commun.* **7**, 11283 (2016).
4. Akselrod, G. M. *et al.* Probing the mechanisms of large Purcell enhancement in plasmonic nanoantennas. *Nat. Photonics* **8**, 835–840 (2014).
5. Boulesbaa, A. *et al.* Ultrafast Dynamics of Metal Plasmons Induced by 2D Semiconductor Excitons in Hybrid Nanostructure Arrays. *ACS Photonics* **3**, 2389–2395 (2016).
6. Santhosh, K. *et al.* Vacuum Rabi splitting in a plasmonic cavity at the single quantum emitter limit. *Nat. Commun.* **7**, ncomms11823 (2016).
7. Schwarz, S. *et al.* Two-Dimensional Metal-Chalcogenide Films in Tunable Optical Microcavities. *Nano Lett.* **14**, 7003–7008 (2014).
8. Deng, H., Weihs, G., Santori, C., Bloch, J. & Yamamoto, Y. Condensation of Semiconductor Microcavity Exciton Polaritons. *Science*. **298**, 199-202 (2002).
9. Kasprzak, J. *et al.* Bose-Einstein condensation of exciton polaritons. *Nature* **443**, 409–414 (2006).
10. Christmann, G., Butté, R., Feltin, E., Carlin, J.-F. & Grandjean, N. Room temperature polariton lasing in a GaN/AlGaIn multiple quantum well microcavity. *Appl. Phys. Lett.* **93**, 51102 (2008).
11. Carusotto, I. & Ciuti, C. Quantum fluids of light. *Rev. Mod. Phys.* **85**, 299–366 (2013).
12. Ballarini, D. *et al.* All-optical polariton transistor. *Nat. Commun.* **4**, 1778 (2013).
13. Dreismann, A. *et al.* A sub-femtojoule electrical spin-switch based on optically trapped polariton condensates. *Nat. Mater.* **15**, 1074–1078 (2016).
14. Sanvitto, D. & Kéna-Cohen, S. The road towards polaritonic devices. *Nat. Mater.* **15**, 1061–1073 (2016).
15. Sidler, M. *et al.* Fermi polaron-polaritons in charge-tunable atomically thin semiconductors. *Nat. Phys.* **13**, 255–261 (2017).
16. Dufferwiel, S. *et al.* Exciton-polaritons in van der Waals heterostructures embedded in tunable microcavities. *Nat. Commun.* **6**, 8579 (2015).
17. Lee, B. *et al.* Fano Resonance and Spectrally Modified Photoluminescence Enhancement in Monolayer MoS₂ Integrated with Plasmonic Nanoantenna Array. *Nano Lett.* **15**, 3646–3653 (2015).
18. Lundt, N. *et al.* Room-temperature Tamm-plasmon exciton-polaritons with a WSe₂ monolayer. *Nat. Commun.* **7**, 13328 (2016).

19. Flatten, L. C. *et al.* Room-temperature exciton-polaritons with two-dimensional WS₂. *Sci. Rep.* **6**, 33134 (2016).
20. Chikkaraddy, R. *et al.* Single-molecule strong coupling at room temperature in plasmonic nanocavities. *Nature* **535**, 127–130 (2016).
21. Benz, F. *et al.* Single-molecule optomechanics in ‘picocavities’. *Science* **354**, 726 (2016).
22. de Nijs, B. *et al.* Unfolding the contents of sub-nm plasmonic gaps using normalising plasmon resonance spectroscopy. *Faraday Discuss.* **178**, 185 (2015).
23. Sigle, D. O. *et al.* Monitoring Morphological Changes in 2D Monolayer Semiconductors Using Atom-Thick Plasmonic Nanocavities. *ACS Nano* **9**, 825 (2015).
24. Schuller, J. A. *et al.* Orientation of luminescent excitons in layered nanomaterials. *Nat. Nanotechnol.* **8**, 271 (2013).
25. Zengin, G. *et al.* Approaching the strong coupling limit in single plasmonic nanorods interacting with J-aggregates. *Sci. Rep.* **3**, 83–90 (2013).
26. Roller, E.-M., Argyropoulos, C., Högele, A., Liedl, T. & Pilo-Pais, M. Plasmon–Exciton Coupling Using DNA Templates. *Nano Lett.* **16**, 5962–5966 (2016).
27. Melnikau, D. *et al.* Rabi Splitting in Photoluminescence Spectra of Hybrid Systems of Gold Nanorods and J-Aggregates. *J. Phys. Chem. Lett.* **7**, 354–362 (2016).
28. Zeng, H. & Cui, X. An optical spectroscopic study on two-dimensional group-VI transition metal dichalcogenides. *Chem. Soc. Rev.* **44**, 2629–2642 (2015).
29. Palumbo, M., Bernardi, M. & Grossman, J. C. Exciton radiative lifetimes in two-dimensional transition metal dichalcogenides. *Nano Lett.* **15**, 2794–2800 (2015).
30. Akselrod, G. M. *et al.* Leveraging Nanocavity Harmonics for Control of Optical Processes in 2D Semiconductors. *Nano Lett.* **15**, 3578–3584 (2015).
31. Chikkaraddy, R. *et al.* How Ultranarrow Gap Symmetries Control Plasmonic Nanocavity Modes: From Cubes to Spheres in the Nanoparticle-on-Mirror. *ACS Photonics* (2017). doi:10.1021/acsp Photonics.6b00908
32. Benz, F. *et al.* Nanooptics of Molecular-Shunted Plasmonic Nanojunctions. *Nano Lett.* **15**, 669–674 (2015).
33. Milonni, P. W. Field Quantization and Radiative Processes in Dispersive Dielectric Media. *J. Mod. Opt.* **42**, 1991–2004 (1995).
34. Liang, W. Y., Beal, A. R., Knights, J. Hughes, H. P. & Bayliss, S. C. Optical anisotropy in layer compounds. *J. Phys. C Solid State Phys* **6**, 551–565 (1973).
35. Arora, A. *et al.* Excitonic resonances in thin films of WSe₂ : from monolayer to bulk material. *Nanoscale* **7**, 10421–10429 (2015).
36. Zhao, W. *et al.* Origin of indirect optical transitions in few-layer MoS₂, WS₂, and WSe₂. *Nano Lett.* **13**, 5627–5634 (2013).
37. Selig, M. *et al.* Excitonic linewidth and coherence lifetime in monolayer transition metal dichalcogenides. *Nat. Commun.* **7**, 13279 (2016).
38. Wang, S. *et al.* Coherent coupling of WS₂ monolayers with metallic photonic nanostructures at room temperature. *Nano Lett.* **16**, 4368–4374 (2016).
39. Benz, F. *et al.* Generalized circuit model for coupled plasmonic systems. *Opt. Express* **23**, 33255 (2015).
40. Fauchaux, J. A., Fu, J. & Jain, P. K. Unified Theoretical Framework for Realizing Diverse Regimes of Strong Coupling between Plasmons and Electronic Transitions. *J. Phys. Chem. C* **118**, 2710–2717 (2014).
41. Mertens, J. *et al.* Tracking optical welding through groove modes in plasmonic nano-

- cavities. *Nano Lett.* **16**, 5605 (2016).
42. Deng, H., Haug, H. & Yamamoto, Y. Exciton-polariton Bose-Einstein condensation. *Rev. Mod. Phys.* **82**, 1489–1537 (2010).
 43. Liu, X. *et al.* Strong light–matter coupling in two-dimensional atomic crystals. *Nat. Photonics* **9**, 30–34 (2015).
 44. Dintinger, J., Klein, S., Bustos, F., Barnes, W. L. & Ebbesen, T. W. Strong coupling between surface plasmon-polaritons and organic molecules in subwavelength hole arrays. *Phys. Rev. B* **71**, 35424 (2005).
 45. Peter, G. *et al.* Linewidth Dependence of Radiative Exciton Lifetimes in Quantum Wells. **59**, 2337 (1987).
 46. Shi, H., Pan, H., Zhang, Y.-W. & Yakobson, B. I. Quasiparticle band structures and optical properties of strained monolayer MoS₂ and WS₂. *Phys. Rev. B* **87**, (2013).
 47. For larger nanoparticles such as cubes 29 where the cube side (75nm) separates opposite phase driving, this exceeds d_c and allows weak coupling to the exciton through s_{11} .
 48. Liang, W. Y. Optical anisotropy in layer compounds. *J. Phys. C Solid State Phys* **6**, 551–565 (1973).
 49. Benz, F. *et al.* SERS of Individual Nanoparticles on a Mirror: Size Does Matter, but so Does Shape. *J. Phys. Chem. Lett.* **7**, (2016).
 50. Kleemann, M.-E. *et al.* Revealing Nanostructures through Plasmon Polarimetry. *ACS Nano* **11**, 850–855 (2017).